Research Square

Preprints are preliminary reports that have not undergone peer review.
They should not be considered conclusive, used to inform clinical practice,
or referenced by the media as validated information.

Altered resting-state functional connectivity and network topology in early-stage Parkinson's disease: associations with depressive symptoms

Zahra Khandan Khadem-Reza
Mashhad University of Medical Sciences
Mohammad Amin Shahram
Sabzevar University of Medical Sciences
Seyed Amin Ghaemmaghami
Mashhad University of Medical Sciences
Alireza Montazerabadi
Mashhad University of Medical Sciences
Mahtab Khajeh
Sabzevar University of Medical Sciences
Seyedehhoda Khatibmasjedi
Case Western Reserve University, University Hospitals, Seidman Cancer Center
Hoda Zare
zareh@mums.ac.ir

Mashhad University of Medical Sciences

Research Article

Keywords: Parkinson's disease, Resting-state functional magnetic resonance imaging (rs-fMRI), Graph theory

Posted Date: July 10th, 2026

DOI: https://doi.org/10.21203/rs.3.rs-10114282/v1

License: This work is licensed under a Creative Commons Attribution 4.0 International License. Read Full License

Additional Declarations: No competing interests reported.

Abstract

Introduction:

Parkinson's disease (PD) is one of the most common neurodegenerative disorders, affecting approximately 1–2% of people over 60 years of age worldwide. Early diagnosis of PD from other neurodegenerative diseases remains challenging due to the lack of reliable biomarkers. Further research is needed to discover sensitive and reliable biomarkers for PD. Resting-state functional magnetic resonance imaging (rs-fMRI), as a non-invasive imaging method, provides valuable information about changes in functional brain connectivity and brain networks in PD. In addition to measuring spontaneous brain activity, studies have shown that the connectivity profile within or between important brain networks is also altered and disrupted. Therefore, this study aims to investigate alterations in functional connectivity and graph-theoretical network properties in early-stage PD compared to healthy controls.

Materials and Methods

Structural magnetic resonance imaging (sMRI) and rs-fMRI of 35 patients with PD and 22 healthy controls, along with demographic information, and psychological test results (GD-Scale) were collected from the PPMI database. CONN software was used for preprocessing, noise removal, and extracting functional connectivity matrix and graph parameters. Finally, by extracting the functional matrix and graph parameters, the rs-fMRI images of the two PD and control groups were statistically compared. The correlation between depressive symptom severity (measured by the Geriatric Depression Scale, GDS) and rs-fMRI features was also examined.

Results

The statistical results of this study showed that in patients with PD, functional connectivity decreased in the left and right Postcentral Gyrus regions. At the same time, it increased in the right and left Insular Cortex regions and the left Planum Temporale. Examination of graph parameters revealed decreased global efficiency and degree centrality, but increased average path length, in the default mode network of PD patients compared to controls.

Conclusion

These findings suggest that rs-fMRI may reveal network-level alterations associated with early-stage PD, particularly in relation to depressive symptoms, though diagnostic applications require further validation.

1. Introduction

Parkinson's disease (PD) is a neurodegenerative disorder primarily characterized by bradykinesia, tremor, and rigidity. PD is the second most common neurodegenerative disorder affecting approximately 1–3% of individuals over 80 years old (1, 2). PD is also more common in men than in women. PD is estimated to have an average duration of 4.9 years and a 2.9-fold increased mortality compared to age-matched healthy individuals and women present decreased survival compared to men (3, 4). PD diagnosis is typically confirmed after significant neuronal degeneration, highlighting the need for early detection. The progressive loss of midbrain area dopamine neurons, particularly in the substantia nigra, is responsible for the cardinal movement symptoms of PD, including tremor, rigidity, bradykinesia, and postural instability. Understanding the neurobiological basis of PD and its clinical markers is critical for improving diagnostic accuracy and therapeutic strategies. Early identification of PD biomarkers is crucial for timely intervention and better patient outcomes. (5, 6). Several clinical scales assess motor dysfunction and disability in PD subjects. But indeed, most of these scales are never formally validated, and cannot be retraced to neurobiological determinants of PD or to linked nominated brain regions. Furthermore, their outcomes often depend on the clinician's ability (7, 8). The Hoehn and Yahr scale is commonly used to compare patient populations and to grade the progression of the disease; ranges from 0 (no symptoms) to 5 (advanced disease). The Unified PD Rating Scale (UPDRS) is routinely used to assess disability and central nervous system degeneration in PD patients. PD(8, 9). The Geriatric Depression Scale (GDS) is another tool used to assess the severity of

depression in PD patients. Despite these tools, PD diagnosis is still primarily based on clinical criteria, and no definitive laboratory test exists for its confirmation (10).

Recently, advanced neuroimaging techniques, especially resting-state functional magnetic resonance imaging (rs-fMRI), enabled further understanding of perceptive functional connection in patients with PD (11). Blood-oxygenation level-dependent (BOLD) signals are utilized in rs-fMRI as a neurophysiological index to probe brain activity and connectivity between brain regions. The whole-brain system investigation of the neuropathological underpinnings of many neurological and psychiatric disorders can be done using the BOLD signals as a proficient and non-invasive strategy (12–15). Previous resting-state fMRI studies in PD have largely emphasized the default mode network (DMN) and motor-related regions as key loci of disruption (16, 17). However, converging evidence shows that alterations extend beyond these networks. For instance, Franciotti et al. (2019) (18) reported cerebellar and salience network dysfunctions, while Yeager et al. (2023) (19) highlighted widespread alterations involving attention and visual networks. Therefore, rather than assuming these networks have been overlooked, the novelty of our study lies in its integrative design, in which we simultaneously assess inter-network connectivity and global topological properties of brain networks using graph theory. This dual-level approach provides a systems-level characterization of PD-related alterations that complements prior network-specific or graph-theoretical studies. While these networks have been examined in isolation in prior work, few studies have adopted a unified framework that integrates whole-brain graph metrics with inter-network connectivity in early-stage PD. Moreover, unlike most studies that have focused on older populations, this research includes a younger age group. In this study, early-stage PD is defined as Hoehn & Yahr stage ≤ 2, disease duration < 2 years, and UPDRS part III (off) score < 30. By studying individuals at an earlier stage of the disease, we aim to contribute to the early detection of PD, which is crucial for implementing effective interventions before significant clinical symptoms appear. Early diagnosis can lead to improved management strategies and a better quality of life for patients. Additionally, this study explores the correlation between rs-fMRI features and depressive symptom severity, as measured by the Geriatric Depression Scale (GDS)—a common non-motor comorbidity in PD. This approach not only enhances our understanding of the brain regions affected by the disease but also paves the way for designing more personalized treatment plans that consider both neural biomarkers and clinical manifestations of PD. In summary, this study contributes to the growing body of literature by examining the functional connectivity of multiple brain networks in PD, focusing on underexplored networks and younger patients, and correlating these features with depressive symptom severity to advance our understanding of network-level alterations in early-stage PD.

2. Materials and methods

2.1. Data acquisition

In this study, Structural Magnetic Resonance Imaging (sMRI) and rs-fMRI data from 35 patients with PD and 22 healthy controls were used, along with their psychological test results based on the Geriatric Depression Scale (GDS). These data were acquired using a Siemens Trio Tim 3 Tesla scanner. The GDS is a standardized test designed to evaluate the level of depression in individuals, with scores ranging from 0 to 15; higher scores indicate more severe depression. The demographic characteristics of all participants are presented in Table 1 .The imaging and clinical data were selected and downloaded from the Parkinson's Progression Markers Initiative (PPMI) database, a widely recognized and reliable resource providing comprehensive neuroimaging and clinical datasets for PD research. The Inclusion criteria for this study were availability of both sMRI and rs-fMRI data, as well as complete GDS test scores. Subjects with missing scans, poor image quality due to motion artifacts, or incomplete clinical or psychological assessments were excluded. All PD participants met criteria for early-stage disease: Hoehn & Yahr stage ≤ 2, disease duration < 2 years from diagnosis, and UPDRS part III (off medication) score < 30. The final dataset was curated to ensure high data quality and completeness across modalities for robust and reliable analysis. sMRI was acquired with a voxel size of 1 × 1 × 1 mm^3, matrix size of 256 × 256, and 176 slices, yielding a FOV of 256 × 256 × 176 mm^3. Rs-fMRI data were acquired with a voxel size of 3 × 3 × 3 mm^3, matrix size of 64 × 64, 48 slices, and a FOV of 192 × 192 × 144 mm^3, using BOLD Echo Planar Imaging (EPI) sequences.

Table 1
Demographics of participants.

Features	Parkinson	Control
Number	35	22
Gender	27M/8F	17M/5F
Age (Year) (Mean ± SD)	62.26 ± 3.53	61.56 ± 5.33
GDS score (Mean)	2.27	1.4
Disease duration (years) (Mean ± SD)	1.4 ± 0.6	-
Hoehn & Yahr stage (Mean ± SD)	1.6 ± 0.5	-
UPDRS-III (off) (Mean ± SD)	22.3 ± 5.1	-
M: Male, F: Female, GD: Geriatric Depression		

2.2. Preprocessing of rs-fMRI brain images

Preprocessing of rs-fMRI brain images was performed using the CONN functional connectivity toolbox (version 20, CONN20) in MATLAB R2019a with the Statistical Parametric Mapping 12 (version 12, SPM12) installed. The preprocessing steps in the CONN20 software were as follows:

2.2.1. Realign and unwarp

In this step, all images were realigned to the first image of each subject's time series, using the B-spline interpolation algorithm. This algorithm can also correct for motion-related distortions. Since double-echo images were not available in this dataset, the Susceptibility Distortion Correction (SDC) algorithm was not applied, which resamples functional data in the phase-encoding direction and corrects field non-uniformities.

2.2.2. Slice-timing correction

Slice timing differences within a Time of Repetition (TR), which are intrinsic to EPI, are corrected using the Spanning Tree Covering (STC) algorithm in the SPM12 toolbox. The functional data were shifted to the middle of the acquisition time.

2.2.3. Outlier identification

The BOLD signals at each time point are checked, and signals showing greater intensity changes than 5 times the standard deviation are removed. Outliers were flagged based on BOLD signal intensity (> 5 SD) or estimated motion (using framewise displacement, FD > 0.5). For denoising, a conservative strategy was applied, which involves strict thresholds for motion and physiological noise removal. This approach retains high-quality BOLD signals while minimizing spurious correlations, following CONN20 toolbox recommendations (20).

2.2.4. Normalization to MNI space

Functional images were co-registered to the high-resolution T1-weighted structural image, and both were normalized to Montreal Neurological Institute (MNI) standard space using unified segmentation as implemented in SPM12.

2.2.5. Smoothing

In this step, functional images were smoothed using a Gaussian kernel with a full width at half maximum (FWHM) of 5 mm to increase the signal-to-noise ratio.

2.2.6. Denoising

To further improve data quality, denoising was performed as the final step of the preprocessing pipeline. In this process, confounding signals from white matter and cerebrospinal fluid (CSF) were identified and removed as covariates using the CONN20 toolbox. Additionally, 12 motion-related noise components were regressed out. Band-pass filtering was applied to remove physiological noise such as cardiac and respiratory fluctuations, retaining only frequencies between 0.008 Hz and 0.09 Hz. Outliers

detected during earlier preprocessing steps were also scrubbed during this stage. To assess the effectiveness of denoising, the distribution of functional connectivity values between Region-of-Interest (ROI) pairs was examined before and after denoising. Prior to denoising, functional connectivity values exhibited a broader distribution with a positive bias; after denoising, the distribution became more centered and narrower, indicating effective noise reduction. Figure 1 illustrates the impact of the denoising process.

2.3. Quality control

After preprocessing, all data underwent rigorous quality control. Functional and structural images were visually inspected for artifacts such as motion, ghosting, or signal dropout. Additionally, the CONN20 toolbox's QC pipeline was used to compute framewise displacement (FD) and global BOLD signal change. Outlier scans were identified using thresholds of FD > 0.5 mm or global signal change exceeding 3 SD. Subjects with more than 20% outlier volumes were excluded. This ensured that only high-quality datasets proceeded to the denoising and analysis steps.

2.4. Brain network

A network consists of nodes and edges in which the nodes represent fundamental components within a system, and edges indicate the connections between these nodes (21). This study utilized the Harvard-Oxford atlas (HOA), which comprises 132 cortical and subcortical regions. Functional connectivity in the brain network refers to the temporal correlation of BOLD signals between each pair of segmented brain regions. For each individual, the time series in each ROI was obtained by averaging the time series of all voxels within that region. In this step, the average time series corresponding to the 132 brain regions of the HOA are extracted for each participant using the CONN20 toolbox by selecting the first-level analysis option. To measure the correlations between these regions, various methods can be employed. In this study, to compute these coefficients for an individual, the mean BOLD signal of the voxels in each region was first calculated. Then, by compiling all full-brain volume images of the same individual, the time-series signal for these regions was obtained. Subsequently, pairwise Pearson correlation coefficients (PCC) were computed between the 132 regional time series to construct a 132×132 functional connectivity matrix for each participant (22).

Each off-diagonal element (i,j) of the matrix represents the PCC between the average BOLD time series of region i and region j. Diagonal elements are 1 (perfect self-correlation), and the matrix is symmetric due to the commutative property of correlation. PCC values range from − 1 to + 1. Figure 2 shows the correlation matrix for a representative Parkinson's patient.

2.4.1. Brain Graph Analysis

The human brain, as a complex network, can be modeled using graphs where nodes represent brain regions and edges indicate the connections between these regions (23). Brain graphs provide valuable insights into the topology, connectivity, and centrality properties of the network. In this study, brain graphs were constructed for each individual using correlation matrices derived from BOLD signals. These analyses were conducted using the CONN20 software, and graph parameters were calculated at the whole-brain level. In addition to whole-brain graph analysis, functional brain networks were also examined. Functional networks were defined using the Harvard–Oxford atlas (HOA), which provides a standard parcellation of 132 cortical and subcortical regions. These regions were grouped into eight canonical functional networks based on established network templates implemented in the CONN20 toolbox. These networks included the Default Mode Network (DMN), Sensorimotor Network (SMN), Visual Network (VN), Posterior Attention Network (PAN), Salience Network (SN), Central Executive Network (CEN), Auditory Network (AN), and Language Network (LN). For each network, relevant nodes and edges were extracted from the correlation matrices, and similar analyses were performed. The results revealed functional and connectivity differences in brain networks between Parkinson's patients and the control group.

To assess inter-network connectivity, the BOLD time series of all ROIs belonging to each canonical network (e.g., DMN, SN) were averaged to obtain a single representative time course per network. Pearson correlations between these network-level time courses were then computed, yielding an 8×8 inter-network connectivity matrix.

2.5. Feature extraction

Feature extraction from rs-fMRI images was performed in two stages. In the first stage, PCCs were calculated from the functional connectivity matrix to assess the increase or decrease in functional connectivity between each pair of brain regions (132 regions from the HOA). In the second stage, after selecting the relevant nodes corresponding to the desired networks and chosen atlas, the

corresponding graph is constructed. Subsequently, the nodal and global parameters of the undirected weighted graph for the entire brain, as well as the global parameters of the undirected weighted graphs for the selected networks, are extracted.

Functional connectivity between each pair of ROIs was calculated using Pearson correlation coefficients, implemented in the CONN20 toolbox in MATLAB. After constructing the functional connectivity graphs, graph theory metrics including degree centrality, average path length, global efficiency, and network cost were automatically extracted by the software for each subject. Degree centrality quantifies the importance of individual nodes in maintaining network communication. Average path length reflects the average shortest path between nodes; longer paths indicate less efficient information transfer. Global efficiency, defined as the average inverse of path length, measures overall network integration. Network cost indicates the proportion of potential connections that are realized, reflecting network organization and potential compensatory changes in Parkinson's disease. Graph theory metrics including degree centrality, average path length, global efficiency, and network cost were automatically extracted by the software for each subject. All graph-theoretical features used in this study are defined in Table 2.

Table 2
Graph theory metrics and ROI-to-ROI correlation, computed using the CONN20 toolbox in MATLAB

Feature	Description
PCC (X,Y) (X = 1:132, Y = 1:132)	Pearson correlation coefficient between each pair of Fisher functional connections matrix region. Quantifies the degree to which nodes in a network tend to form local clusters or interconnected groups. In brain networks, a higher clustering coefficient reflects stronger local segregation and specialized processing within subnetworks, whereas lower values may indicate disrupted local connectivity often observed in neurodegenerative conditions such as Parkinson's disease.
Degree n (n = 1: 132)	Represents the number of edges connected to the node.
Cost n (n = 1: 132)	The ratio of the number of edges to the specific node.
Average path length n (n = 1: 132)	The average shortest path between the node and all other nodes.
Betweenness Centrality n (n = 1: 132)	The fraction of shortest paths in the graph that pass through the given node.
Clustering Coefficient	The average clustering coefficient of all nodes.
Global Efficiency	The average inverse shortest path length in the graph, indicating the efficiency of information exchange in the graph.
Local Efficiency	The inverse shortest path length in the graph for each region.

PCC: Pearson correlation coefficients

2.6. Statistical analysis

Statistical analyses were conducted using the CONN20 toolbox and p value < 0.05 was considered as a significant level. Normality of each connectivity measure was assessed using the Shapiro–Wilk test. For normally distributed data, independent t-tests were used; otherwise, Mann–Whitney U tests were applied. Multiple comparisons were corrected using the Benjamini–Hochberg procedure with a false discovery rate threshold of q < 0.05. Effect sizes (Cohen's d or r) and exact p-values are reported for all comparisons. To examine the correlation between GDS scores and rs-fMRI features, Spearman's rank correlation test was used.

3. Results

We report rs-fMRI-derived parameters, including functional connectivity matrices and graph metrics, in the following sections. These parameters were extracted to assess the functional connectivity patterns of brain regions and to explore their relationship with clinical indices of PD. The results are analyzed and compared between the patient group and the control group to identify potential biomarkers for early detection and progression monitoring of PD.

3.1. Statistical analysis of Pearson correlations from the correlation matrix

The analysis of PCC derived from the HOA correlation matrix revealed significant differences in functional connectivity between the PD group and the control group. The largest reductions in functional connectivity within the PD group were observed in the Postcentral Gyrus regions. Conversely, the most notable increases in functional connectivity were found in the Insular Cortex Right, Insular Cortex Left, and Planum Temporale Left regions. Table 3 summarizes the regions with significantly increased or decreased functional connectivity in Parkinson's disease patients compared with healthy controls, along with the corresponding statistical tests, exact p-values, and FDR-corrected p-values. Additionally, network-level analyses (reported in Section 3.3) revealed altered within-network connectivity in several canonical networks, including the DMN, CEN, and DAN.

Table 3
Functional Connectivity Changes in Parkinson's Patients Compared to the Control Group.

ROI	Comparison (PD vs. Control)	Direction	p-value	FDR-corrected p
Thalamus	PD > Control	Increased	0.012	0.028
Heschl's Gyrus	PD > Control	Increased	0.009	0.022
Insular Cortex	PD > Control	Increased	0.015	0.031
Central Opercular Cortex	PD > Control	Increased	0.010	0.024
Planum Temporale	PD > Control	Increased	0.013	0.029
Cuneal Cortex	PD > Control	Increased	0.018	0.037
Putamen	PD > Control	Increased	0.011	0.026
Frontal Operculum Cortex	PD > Control	Increased	0.010	0.025
Hippocampus	PD > Control	Increased	0.017	0.034
Parahippocampal Gyrus	PD > Control	Increased	0.014	0.030
Lateral Occipital Cortex	PD > Control	Increased	0.012	0.028
Right Precentral Gyrus	PD > Control	Increased	0.009	0.022
Right Occipital Fusiform Gyrus	PD > Control	Increased	0.016	0.033
Left Lingual Gyrus	PD > Control	Increased	0.010	0.025
Left Occipital Fusiform Cortex	PD > Control	Increased	0.014	0.031
Left Temporal Pole	PD > Control	Increased	0.018	0.037
Postcentral Gyrus	PD < Control	Decreased	0.009	0.024
Middle Frontal Gyrus	PD < Control	Decreased	0.011	0.027
Superior Parietal Lobule	PD < Control	Decreased	0.015	0.032
Cingulate Gyrus	PD < Control	Decreased	0.013	0.029
Vermis 6	PD < Control	Decreased	0.012	0.028
Vermis 7	PD < Control	Decreased	0.016	0.035
Right Cerebellum 9	PD < Control	Decreased	0.011	0.027
Right Cingulate Lobule	PD < Control	Decreased	0.013	0.030
Left Cerebellum Crus I	PD < Control	Decreased	0.010	0.025
Left Cerebellum 9	PD < Control	Decreased	0.019	0.039
Left Cerebellum Crus II	PD < Control	Decreased	0.012	0.029

3.2. Statistical analysis of undirected graph parameters of brain networks

The statistical analysis of undirected graph parameters for functional brain networks revealed significant differences between the PD group and the control group, reflecting alterations in the topological organization of large-scale brain networks in early-stage PD. Detailed results are provided in Table 4.

Degree centrality was significantly increased in the salience network (SN), dorsal attention network (DAN), and visual network (VN) in PD patients compared to controls, while it was decreased in the default mode network (DMN). Average path length was

increased in the DMN (2.50 vs. 2.31), sensorimotor network (SMN), visual network (VN), salience network (SN), dorsal attention network (DAN), and central executive network (CEN), indicating reduced efficiency of information transfer within these networks.

Consistent with this, global efficiency was decreased in the DMN (0.37 vs. 0.54) but increased in the salience network (SN), visual network (VN), language network (LN), and central executive network (CEN). Additionally, network cost—reflecting the proportion of realized connections—was significantly higher in the DAN, VN, and CEN, but lower in the DMN, suggesting a reorganization of network wiring in PD.

In contrast, betweenness centrality, clustering coefficient, and local efficiency did not show statistically significant differences between groups across any of the examined networks.

Table 4
Statistical analysis of undirected graph parameters; significant differences between functional networks of the Parkinson's group and the control group.

Parameter	Network	Value (Parkinson / Control)	P-value	FDR-corrected p
Degree centrality	SN	50.2 / 49.34	0.002	0..004
	DAN	50 / 49.5	0.001	0.003
	DMN	47 / 47.5	0.001	0.004
	VN	51 / 50.83	0.002	0.005
Cost	CEN	0.8 / 0.63	0.002	0.004
	DAN	0.9 / 0.73	0.002	0.005
	DMN	0.8 / 0.97	0.002	0.004
	VN	0.7 / 0.53	0.002	0.003
Average path length	CEN	2.40 / 1.40	0.001	0.004
	DAN	2.27 / 1.27	0.042	0.046
	DMN	2.5 / 2.31	0.001	0.045
	VN	2.34 / 1.34	0.001	0.045
	SN	2.40 / 1.39	0.001	0.004
	SMN	2.31 / 1.31	0.001	0.036
Global efficiency	CEN	0.43 / 0.25	0.042	0.004
	SN	0.36 / 0.19	0.042	0.005
	DMN	0.37 / 0.54	0.002	0.003
	VN	0.41 / 0.24	0.001	0.028
	LN	0.39 / 0.22	0.002	0.003

DMN: Default Mode Network, SMN: SensoriMotor network, VN: Visual Network, PAN: Posterior Attention Network, SN: Salience Network, CEN: Central Executive Network, AN: Auditory network, LN: Language Network

3.3. Correlation analysis of the GD-scale clinical index with rs-fMRI parameters in PD's patients

The correlation between rs-fMRI-derived features and Geriatric Depression Scale (GDS) scores was evaluated using Spearman's rank correlation test. As summarized in Table 5, GDS scores showed significant correlations (FDR-corrected $p < 0.05$) with multiple rs-fMRI features in the PD group. These include global efficiency and average path length in the default mode network (DMN), as well as global efficiency in the dorsal attention network (DAN). Additionally, 31 ROI-to-ROI functional connectivity pairs exhibited

significant associations with GDS scores. Many of these connections involve regions implicated in emotional and limbic processing, such as the cingulate gyrus, hippocampus, and insula.

However, it should be emphasized that the GDS is a general measure of depressive symptoms and not a PD-specific clinical scale. Given that depression is a common non-motor comorbidity in PD and is itself associated with functional connectivity alterations—particularly within the DMN and limbic circuits—the observed correlations may reflect the neural correlates of comorbid mood symptoms rather than core PD pathophysiology. In the absence of statistical control for depression as a confounding variable, these associations should be interpreted with caution. Future studies should employ PD-specific clinical metrics (e.g., MDS-UPDRS) and multivariate models to disentangle disease-related network changes from those driven by depressive symptoms.

Table 5
Correlation of GD-Scale index with resting-state functional magnetic resonance imaging.

Feature	r	P-value	FDR-corrected p	Feature	r	FDR-corrected p	P-value	Feature	r	P-value	FDR-corrected p
Global efficiency	0.296	0.035	0.048	PCC (74,82)	-0.354	0.022	0.011	PCC (36, 39)	0.243	0.002	0.008
PCC (65,71)	0.372	0.007	0.018	PCC (59.62)	-0.325	0.034	0.020	PCC (35, 37)	0.245	0.023	0.041
PCC (2,66)	0.353	0.011	0.025	PCC (1, 6)	-0.404	0.012	0.003	PCC (60,62)	0.690	0.008	0.020
PCC (5,71)	0.413	0.003	0.012	PCC (82,85)	-0.310	0.043	0.027	Average path length	0.312	0.035	0.047
PCC (40,65)	0.457	0.001	0.006	PCC (87,90)	0.309	0.042	0.027	PCC (71,72)	0.323	0.046	0.049
PCC (2, 35)	0.343	0.014	0.028	PCC (2, 6)	0.307	0.044	0.028	PCC (81,85)	0.210	0.009	0.021
PCC (7, 14)	0.356	0.010	0.026	PCC (85,90)	-0.327	0.036	0.019	PCC (1, 31)	0.137	0.035	0.009
PCC (83,88)	0.408	0.003	0.014	PCC (1,65)	0.451	0.048	0.049	PCC (83,87)	0.210	0.049	0.047
PCC (84,40)	0.326	0.020	0.035	PCC (7,72)	0.381	0.046	0.0385	PCC (1, 9)	0.180	0.035	0.045
PCC (7, 13)	0.383	0.006	0.010	PCC (39,41)	0.267	0.018	0.002	PCC (1,66)	0.352	0.001	0.024
PCC (33, 38)	0.309	0.028	0.036	PCC (35, 40)	0.389	0.056	0.025	PCC (56,59)	0.221	0.007	0.023

PCC: Pearson correlation coefficients

4. Discussion

The present study introduces a novel approach by comprehensively examining functional networks associated with PD, including the DMN, SMN, FPN, CN, DAN, LN, VN, and SN. Notably, networks such as the FPN, DAN, LN, and SN have not been explored in prior studies. Additionally, the inclusion of younger participants highlights the potential for early detection and intervention, addressing a

critical gap in previous research. The findings revealed widespread alterations in functional connectivity. Increased connectivity was observed in regions such as the thalamus, insular cortex, putamen, and hippocampus, while decreased connectivity was noted in the cerebellum, postcentral gyrus, and cingulate gyrus. These results provide critical insights into the neural mechanisms underlying motor, sensory, and cognitive symptoms in PD's patients. In this study, increased functional connectivity in the thalamus, a central hub for sensory and motor signal processing, was observed. Given that sensory and motor symptoms are among the primary features of PD, this increase in connectivity is predictable. These findings align with the results of Hu et al.(24), but contrasts with Hacker et al.(25) and Agosta et al.(26). Enhanced connectivity in the insular cortex, a region integral to sensory integration and cognitive processes, was observed in this study. This finding aligns with the results of Wang et al. (27), while contradicting those of Wu et al. (28). These alterations may account for the cognitive impairments frequently observed in PD's patients. In this study, increased connectivity was observed in the putamen, a critical structure for motor coordination, which contrasts with several previous studies (25, 28–30). This increase may reflect compensatory processes; however, this interpretation remains speculative and requires validation in longitudinal or task-based studies. Increased connectivity in the hippocampus and parahippocampal gyrus, regions critical for memory and sensory integration, underscores their involvement in PD's pathology, particularly in sensory and memory impairments. Conversely, reduced connectivity was observed in key motor-related areas, including the cerebellum, vermis, and postcentral gyrus. In our study, decreased connectivity in Crus I, Crus II, and lobule IX of the cerebellum was observed, which is confirmed by Hacker et al. (25) and Ma et al. (31), but contrasts with the findings of Wu et al. (30), highlighting the cerebellum's role in motor coordination and postural stability. Similarly, reduced connectivity in the vermis lobules, crucial for balance and eye movement coordination, highlights the widespread impact of PD on motor systems. Several novel findings were also identified in this study. Increased connectivity in regions such as the occipital fusiform gyrus, Planum Temporale, Heschl's gyrus, and central opercular cortex has not been previously reported in studies. These regions are associated with functions like facial recognition, auditory processing, and cognitive planning, offering new perspectives on PD.

To compare the statistical results of functional connectivity in brain networks from the current study with those of other studies, it was observed that in the DMN, which includes regions such as the medial prefrontal cortex (MPFC) and posterior cingulate cortex (PCC), increased connectivity was observed between the Default Mode-MPFC and Default Mode-PCCThis finding suggests a significant alteration in the connectivity of the DMN in PD. The increased connectivity within this network is consistent with findings suggesting disruptions in the default brain network, which is known to be involved in self-referential thinking and mind-wandering. In the DAN, which includes the superior parietal and superior frontal regions, decreased connectivity was observed. This aligns with prior studies (32) and suggests disruptions in spatial attention and visuomotor coordination, impairments that are commonly seen in Parkinson's patients. Specifically, the most significant reduction in connectivity within the DAN occurred between the Dorsal Attention.IPS r and Dorsal Attention.IPS l. This suggests a disruption in attentional control and visuospatial processing, which are commonly impaired in PD. Similarly, the CEN, primarily involving the mesiofrontal cortex, anterior cingulate, and para-cingulate cortex, also demonstrated reduced connectivity. This finding is consistent with study (33) and reflects deficits in executive functions, such as decision-making and cognitive flexibility, that are hallmark symptoms of PD. Conversely, the SMN exhibited increased connectivity in this study, a finding that aligns with studies (34, 35) but contrasts with studies (27, 36). The SMN encompasses critical regions such as the primary sensorimotor cortex, supplementary motor area, and secondary sensory cortex, which are essential for motor control. The observed increase in connectivity could be interpreted as a compensatory mechanism aimed at addressing motor impairments such as rigidity and tremor, which are characteristic of PD. Changes in the CN were also evident, with reduced connectivity observed in anterior and posterior cerebellar regions. This result is consistent with study (27) and emphasizes the cerebellum's critical role in both motor coordination and higher cognitive functions. Reduced connectivity in the CN could contribute to the postural instability and coordination deficits commonly reported in PD's patients. Interestingly, increased connectivity was noted in the VN, which includes the lateral and superior occipital gyri and the lingual gyrus.This result supports study (34) and suggests that visual processing impairments in PD's patients may precede clinically apparent visual hallucinations. The involvement of visual cortices in early stages of the disease highlights the potential of the VN as a biomarker for early detection. The SN and Language Network also showed increased functional connectivity in this study. The SN, which includes the anterior insula and dorsal anterior cingulate cortex, plays a crucial role in integrating sensory, emotional, and cognitive information. Changes in the SN's connectivity have not been previously reported, making this finding particularly significant. The most pronounced increase in connectivity within the SN occurred between the Salience.RPFC r and Salience.RPFC l, as well as between Salience.RPFC r and Salience.ACC. Similarly, the increased connectivity in the LN, which was also unreported in prior studies, highlights the potential for investigating language processing and cognitive impairments in PD's patients. To date, no research has been conducted to examine the correlation between the GD-Scale clinical index and resting-state MRI features.

Features that are correlated with this index include the overall efficiency and average path length in the DMN, as well as overall efficiency in the DAN. The correlation analysis between functional connectivity and this index reveals a correlation between the clinical index and 31 functional connections in PD's patients. Based on these results, it can be concluded that the GD-Scale clinical index is most strongly correlated with changes in the DMN and DAN. Interestingly, other fields of medicine have demonstrated that features extracted from imaging biomarkers and their correlation with clinical indices can greatly enhance treatment decision-making. For instance, in glioblastoma, meta-analyses have revealed that the number of adjuvant temozolomide cycles is significantly associated with clinical outcomes, suggesting a valuable role of treatment-based indicators in guiding clinical prognosis (37, 38). Furthermore, it can be concluded that the SMN, VN, LN, SN, and CEN are not suitable for predicting the clinical index of PD. However, brain functional connections remain one of the most valuable clinical biomarkers for predicting the clinical index of PD. The importance of parameters derived from graph analysis, when compared to functional connectivity, has lower value in predicting this clinical index. In this study, we applied graph-theoretical analysis and ROI-based functional connectivity to investigate large-scale brain network alterations in Parkinson's disease (PD). Our results demonstrated significant disruptions in global and local network organization, reflected by reduced global efficiency and increased average path length, along with altered connectivity in motor, cognitive, and limbic networks. The decrease in global efficiency suggests impaired information integration across distributed brain regions, while the increase in average path length indicates reduced efficiency of information transfer. From a neurobiological perspective, such alterations may arise from dysfunction of the basal ganglia–cortical loops, which are crucial for both motor execution and higher cognitive processes (39). Moreover, the observed regional increases in connectivity within the insular and temporal cortices may reflect compensatory mechanisms, whereby non-motor regions attempt to maintain functional communication in the face of progressive nigrostriatal degeneration. This compensatory hyperconnectivity, however, coexists with hypoconnectivity in sensorimotor and parietal cortices, which likely underpins the motor and visuospatial deficits commonly observed in PD patients.

Taken together, these findings highlight that PD is not limited to focal basal ganglia pathology, but involves large-scale reorganization of functional brain networks. The convergence of reduced integration, compensatory hyperconnectivity, and disrupted network interactions provides a systems-level perspective on PD pathophysiology.

Alterations in graph metrics are consistent with known PD pathophysiology, including dopaminergic neuron loss and disruption of functional networks. Increased average path length and decreased global efficiency suggest reduced integration, which could contribute to both motor dysfunctions and cognitive impairments. Changes in degree centrality and network cost reflect altered connectivity patterns in attentional and executive networks, potentially representing compensatory mechanisms. These findings emphasize the relevance of graph theoretical analysis in understanding network-level disruptions in Parkinson's disease.

The use of the GDS provides additional insight into the non-motor symptomatology of PD. Depression is one of the most common non-motor manifestations in PD and has been linked to altered connectivity in the default mode network, limbic regions, and prefrontal cortex. Thus, the significant correlations we observed between GDS scores and rs-fMRI features likely reflect meaningful neurobiological relationships rather than spurious associations. These findings align with previous reports highlighting the neural substrates of depressive symptoms in PD.

Importantly, while our analysis focused on univariate graph metrics, future studies should incorporate multivariate or machine learning approaches to identify robust biomarkers for disease progression. Such approaches may help integrate multi-network alterations into predictive models for clinical outcomes. Additionally, longitudinal investigations could clarify whether these network disruptions evolve with disease severity, and whether they may serve as targets for therapeutic interventions.

5. Limitations

This study faced several limitations that should be considered when interpreting the results. Firstly, the lack of access to PD's patients directly led to the use of data from the PPMI database. Secondly, the study was constrained by the limited availability of resting-state functional MRI images paired with structural images, which resulted in a smaller dataset for analysis. These limitations may impact the generalizability of the findings and suggest the need for future studies with larger and more diverse patient populations.

A major limitation is the use of GDS—a non-PD-specific measure—as the primary clinical correlate. Future studies should incorporate PD-specific scales such as UPDRS or MDS-UPDRS to better link imaging biomarkers to motor and non-motor disease severity.

6. Conclusion

In conclusion, this study emphasizes the importance of functional connectivity analysis in understanding PD. By exploring brain network alterations and identifying new findings, it enhances our understanding of the disease's neural mechanisms. The results suggest that rs- fMRI can serve as a promising non-invasive tool for early detection and clinical prediction in PD patients. This research contributes to the growing body of knowledge in the field and paves the way for further studies aiming to improve diagnostic and therapeutic strategies for PD patients.

Declarations

Acknowledgments

The authors would like to thank the Vice-Chancellor of the Research Department at Mashhad University of Medical Sciences for supporting this project.

Funding

This study was supported by Mashhad University of Medical Sciences, Mashhad, Iran. (Grant No. 981424) (Ethics code: IR.MUMS.MEDICAL.REC.1399.042).

Conflicts of Interest

The authors declare that they have no competing interests.

Consent for publication

Not applicable.

Ethical Statement

The authors are accountable for all aspects of the work in ensuring that questions related to the accuracy or integrity of any part of the work are appropriately investigated and resolved.

Authors' contributions

Z.Kh, MA.Sh ; Contributed to conception and design. M.Kh,A.M and S.A.Gh ; Contributed to all experimental work, data and statistical analysis, and interpretation of data. MA.Sh,Z.Kh ; Drafted the manuscript, which was revised by H.Z and S.Kh. All authors read and approved the final manuscript.

Data Availability

The datasets used in this study were obtained from the Parkinson's Progression Markers Initiative (PPMI) database (www.ppmi-info.org/data). Access to the PPMI dataset is restricted and requires registration and approval. The data are not publicly available due to data usage agreements, but are available from the corresponding author upon reasonable request and with permission from PPMI.

References

1. De Lau, L. M., & Breteler, M. M. (2006). Epidemiology of Parkinson's disease. *The Lancet Neurology*, *5*(6), 525–535.
2. Nussbaum, R. L., & Ellis, C. E. (2003). Alzheimer's disease and Parkinson's disease. *New england journal of medicine*, *348*(14), 1356–1364.

3. Morgan, J. C., Currie, L. J., Harrison, M. B., BennettJr, J. P., Trugman, J. M., & Wooten, G. F. (2014). Mortality in Levodopa-Treated Parkinson' s Disease. *Parkinson's Disease*, *2014*(1), 426976.
4. Van Den Eeden, S. K., Tanner, C. M., Bernstein, A. L., Fross, R. D., Leimpeter, A., Bloch, D. A., et al. (2003). Incidence of Parkinson's disease: variation by age, gender, and race/ethnicity. *American journal of epidemiology*, *157*(11), 1015–1022.
5. Halliday, G. M., Leverenz, J. B., Schneider, J. S., & Adler, C. H. (2014). The neurobiological basis of cognitive impairment in Parkinson's disease. *Movement disorders*, *29*(5), 634–650.
6. Pagan, F. L. (2012). Improving outcomes through early diagnosis of Parkinson's disease. *American Journal of Managed Care*, *18*(7), S176.
7. Ebersbach, G., Baas, H., Csoti, I., Müngersdorf, M., & Deuschl, G. (2006). Scales in Parkinson's disease. *Journal of neurology*, *253*, iv32–iv5.
8. Ramaker, C., Marinus, J., Stiggelbout, A. M., & Van Hilten, B. J. (2002). Systematic evaluation of rating scales for impairment and disability in Parkinson's disease. *Movement disorders: official journal of the Movement Disorder Society*, *17*(5), 867–876.
9. Goetz, C. G., Fahn, S., Martinez-Martin, P., Poewe, W., Sampaio, C., Stebbins, G. T., et al. (2007). Movement Disorder Society-sponsored revision of the Unified Parkinson's Disease Rating Scale (MDS-UPDRS): process, format, and clinimetric testing plan. *Movement disorders*, *22*(1), 41–47.
10. Lopez, F. V., Split, M., Filoteo, J. V., Litvan, I., Moore, R. C., Pirogovsky-Turk, E., et al. (2018). Does the Geriatric Depression Scale measure depression in Parkinson's disease? *International journal of geriatric psychiatry*, *33*(12), 1662–1670.
11. Al-Radaideh, A. M., & Rababah, E. M. (2016). The role of magnetic resonance imaging in the diagnosis of Parkinson's disease: a review. *Clinical imaging*, *40*(5), 987–996.
12. Faraj, R., & Zare, H. (2021). Evaluation of white matter tracts in autistic individuals: a review of diffusion tensor imaging studies. *Shahid Sadoughi University of Medical Sciences Journal*, *29*(3), 3539–3555.
13. Khadem-Reza, Z. K., & Zare, H. (2022). Evaluation of brain structure abnormalities in children with autism spectrum disorder (ASD) using structural magnetic resonance imaging. *The Egyptian Journal of Neurology Psychiatry and Neurosurgery*, *58*(1), 135.
14. Khadem-Reza, Z. K., & Zare, H. (2022). Automatic detection of autism spectrum disorder (ASD) in children using structural magnetic resonance imaging with machine vision system. *Middle East Current Psychiatry*, *29*(1), 54.
15. Khandan Khadem-Reza, Z., Shahram, M. A., & Zare, H. (2023). Altered resting-state functional connectivity of the brain in children with autism spectrum disorder. *Radiological Physics and Technology*, *16*(2), 284–291.
16. Prajapati, R., & Emerson, I. A. (2021). Global and regional connectivity analysis of resting-state function MRI brain images using graph theory in Parkinson's disease. *International Journal of Neuroscience*, *131*(2), 105–115.
17. Sang, L., Zhang, J., Wang, L., Zhang, J., Zhang, Y., Li, P., et al. (2015). Alteration of brain functional networks in early-stage Parkinson's disease: a resting-state fMRI study. *PloS one*, *10*(10), e0141815.
18. Franciotti, R., Pizzi, S. D., Russo, M., Carrarini, C., Carrozzino, D., Perfetti, B., et al. (2019). Somatic symptoms disorders in Parkinson's disease are related to default mode and salience network dysfunction. *NeuroImage: Clinical*, *23*, 101932.
19. Yeager, B. E., Twedt, H. P., Bruss, J., Schultz, J., & Narayanan, N. S. (2024). Cortical and subcortical functional connectivity and cognitive impairment in Parkinson's disease. *NeuroImage: Clinical*, *42*, 103610.
20. Whitfield-Gabrieli, S., & Nieto-Castanon, A. (2012). Conn: a functional connectivity toolbox for correlated and anticorrelated brain networks. *Brain connectivity*, *2*(3), 125–141.
21. Stanley, M. L., Moussa, M. N., Paolini, B. M., Lyday, R. G., Burdette, J. H., & Laurienti, P. J. (2013). Defining nodes in complex brain networks. *Frontiers in computational neuroscience*, *7*, 169.
22. Asuero, A. G., Sayago, A., & González, A. (2006). The correlation coefficient: An overview. *Critical reviews in analytical chemistry*, *36*(1), 41–59.
23. Khazaee, A., Ebrahimzadeh, A., & Babajani-Feremi, A. (2015). Identifying patients with Alzheimer's disease using resting-state fMRI and graph theory. *Clinical Neurophysiology*, *126*(11), 2132–2141.
24. Hu, X., Song, X., Yuan, Y., Li, E., Liu, J., Liu, W., et al. (2015). Abnormal functional connectivity of the amygdala is associated with depression in Parkinson's disease. *Movement Disorders*, *30*(2), 238–244.
25. Hacker, C. D., Perlmutter, J. S., Criswell, S. R., Ances, B. M., & Snyder, A. Z. (2012). Resting state functional connectivity of the striatum in Parkinson's disease. *Brain*, *135*(12), 3699–3711.

26. Agosta, F., Canu, E., Stefanova, E., Sarro, L., Tomić, A., Špica, V., et al. (2014). Mild cognitive impairment in Parkinson's disease is associated with a distributed pattern of brain white matter damage. *Human brain mapping*, *35*(5), 1921–1929.
27. Wang, S., Zhang, Y., Lei, J., & Guo, S. (2021). Investigation of sensorimotor dysfunction in Parkinson disease by resting-state fMRI. *Neuroscience Letters*, *742*, 135512.
28. Wu, T., Long, X., Wang, L., Hallett, M., Zang, Y., Li, K., et al. (2011). Functional connectivity of cortical motor areas in the resting state in Parkinson's disease. *Human brain mapping*, *32*(9), 1443–1457.
29. Manza, P., Zhang, S., Li, C. S. R., & Leung, H. C. (2016). Resting-state functional connectivity of the striatum in early-stage P arkinson's disease: Cognitive decline and motor symptomatology. *Human brain mapping*, *37*(2), 648–662.
30. Wu, T., Wang, L., Chen, Y., Zhao, C., Li, K., & Chan, P. (2009). Changes of functional connectivity of the motor network in the resting state in Parkinson's disease. *Neuroscience letters*, *460*(1), 6–10.
31. Ma, C., Liu, Y., Neumann, S., & Gao, X. (2017). Nicotine from cigarette smoking and diet and Parkinson disease: a review. *Translational neurodegeneration*, *6*, 1–7.
32. Baggio, H. C., Segura, B., Sala-Llonch, R., Marti, M. J., Valldeoriola, F., Compta, Y., et al. (2015). Cognitive impairment and resting-state network connectivity in P arkinson's disease. *Human brain mapping*, *36*(1), 199–212.
33. Amboni, M., Tessitore, A., Esposito, F., Santangelo, G., Picillo, M., Vitale, C., et al. (2015). Resting-state functional connectivity associated with mild cognitive impairment in Parkinson’s disease. *Journal of neurology*, *262*, 425–434.
34. De Schipper, L. J., Hafkemeijer, A., Van der Grond, J., Marinus, J., Henselmans, J. M., & Van Hilten, J. J. (2018). Altered whole-brain and network-based functional connectivity in Parkinson's disease. *Frontiers in neurology*, *9*, 419.
35. Tuovinen, N., Seppi, K., de Pasquale, F., Müller, C., Nocker, M., Schocke, M., et al. (2018). The reorganization of functional architecture in the early-stages of Parkinson's disease. *Parkinsonism & related disorders*, *50*, 61–68.
36. Tessitore, A., Giordano, A., De Micco, R., Caiazzo, G., Russo, A., Cirillo, M., et al. (2016). Functional connectivity underpinnings of fatigue in Drug-Naïve patients with Parkinson's disease. *Movement Disorders*, *31*(10), 1497–1505.
37. Attarian, F., Taghizadeh-Hesary, F., Fanipakdel, A., Javadinia, S. A., Porouhan, P., PeyroShabany, B., et al. (2021). A systematic review and meta-analysis on the number of adjuvant temozolomide cycles in newly diagnosed glioblastoma. *Frontiers in oncology*, *11*, 779491.
38. Shahram, M. A., Azimian, H., Abbasi, B., Ganji, Z., Khadem-Reza, Z. K., Khakshour, E., et al. (2024). Automated glioblastoma patient classification using hypoxia levels measured through magnetic resonance images. *BMC neuroscience*, *25*(1), 26.
39. Olde Dubbelink, K. T., Hillebrand, A., Stoffers, D., Deijen, J. B., Twisk, J. W., Stam, C. J., et al. (2014). Disrupted brain network topology in Parkinson’s disease: a longitudinal magnetoencephalography study. *Brain*, *137*(1), 197–207.
40. Baggio, H. C., Sala-Llonch, R., Segura, B., Marti, M. J., Valldeoriola, F., Compta, Y., et al. (2014). Functional brain networks and cognitive deficits in Parkinson's disease. *Human brain mapping*, *35*(9), 4620–4634.

Figures

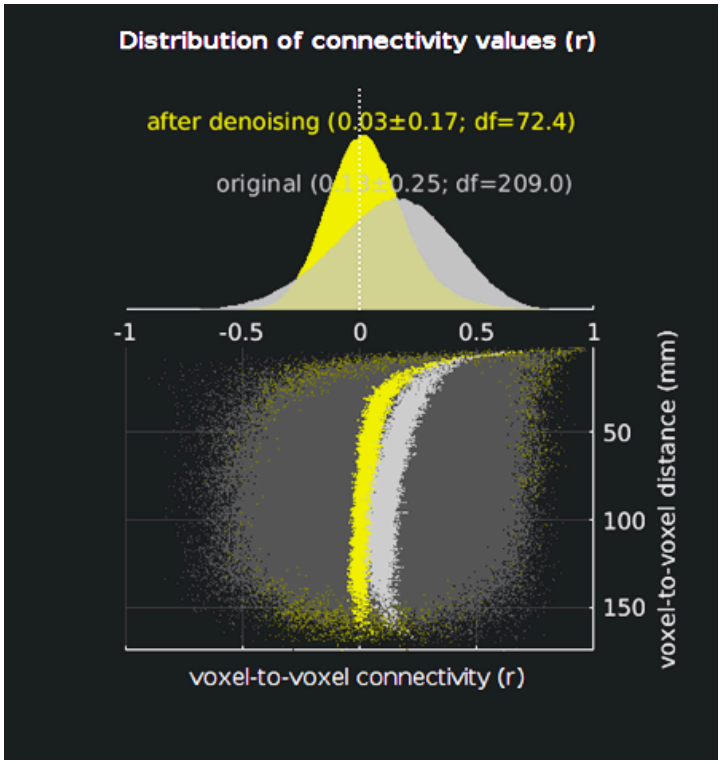


Figure 1

The distribution of functional connectivity values between ROI pairs before and after denoising.

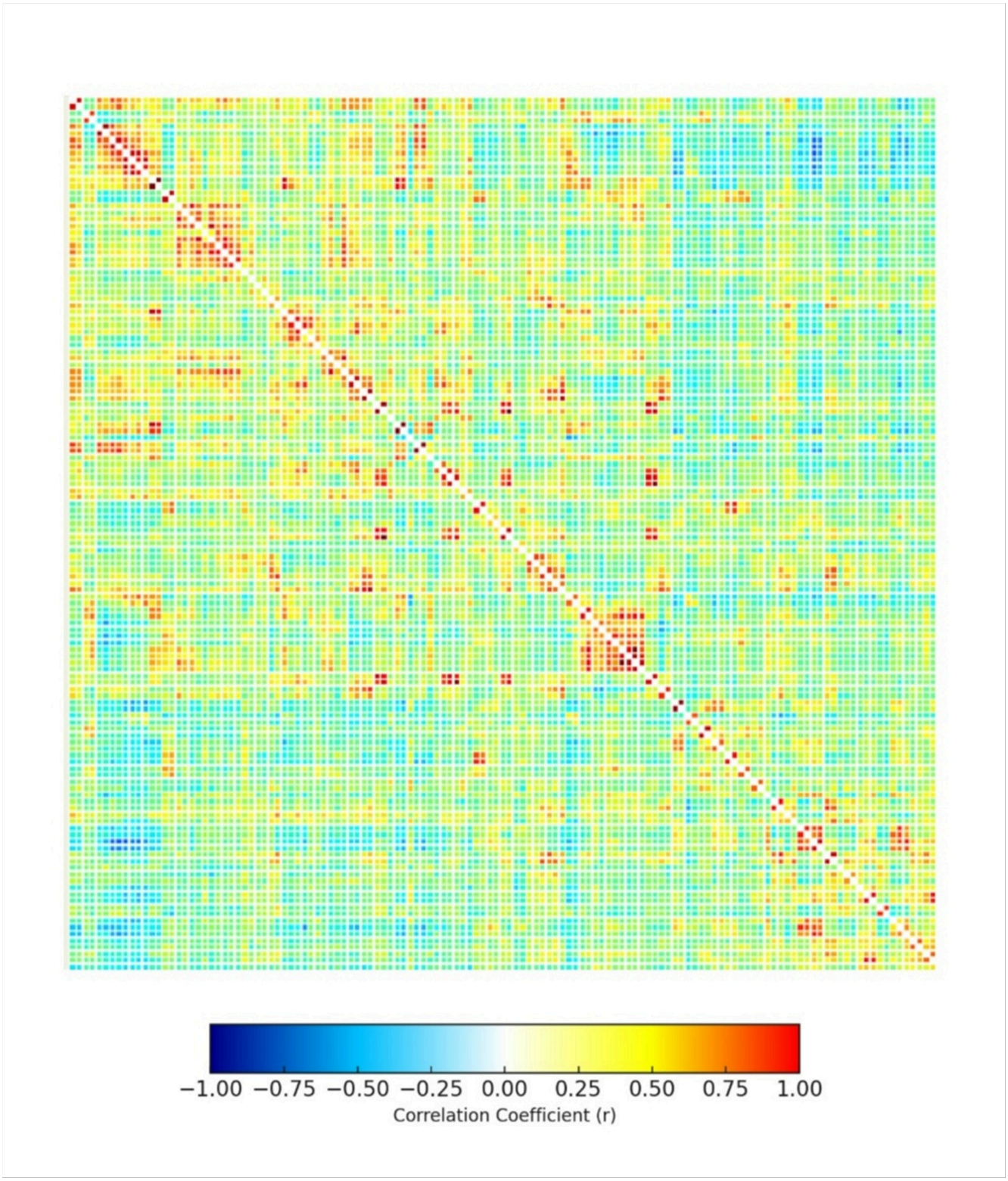


Figure 2

The correlation matrix for a representative Parkinson's patient. The color scale indicates Pearson correlation values, ranging from –1 (blue, negative correlation) to +1 (red, positive correlation)